SCANNING VOL. 25, 230–239 (2003)

Received: March 26, 2003
Accepted with revision: July 16, 2003

Calibration and Quantification of Fast Intracellular Motion (FIM) in Living Cells Using Correlation Analysis

PAVEL VESELY, ANTONÍN MIKŠ,* JIŘÍ NOVÁK,* ALAN BOYDE†

Institute of Molecular Genetics, AS CR; *Department of Physics, Faculty of Civil Engineering, Czech Technical University, Prague, Czech Republic; †Department of Anatomy and Developmental Biology, UC London, London, U.K.

Summary: Video rate confocal laser scanning microscopy at the highest spatial and temporal resolution of backscattered light (BSL) imaging allowed for regular observation of fast intracellular motion (FIM) first revealed in living neoplastic cells. However, the absence of an objective evaluation has hampered further study of the mechanisms and biological significance of FIM. Particularly, a quantification of apparent differences in velocities that would complement and improve the current demonstration of FIM by color coding using the combination of red-green-blue (RGB) images had been missing. Standard methods of tracking or pattern recognition could not be applied because of the fuzzy nature of images of FIM. A search for a suitable method led to correlation analysis. It was calibrated on Brownian motion and a known type of motion, such as cell marginal ruffling, compared with FIM. Results approved its explanatory potential. Therefore, several crucial incidences of FIM could be analyzed. Apart from an argument against viewing FIM as a manifestation of simple Brownian motion, the correlation analysis of FIM in the adjacent peripheries of a rat fibroblast and a K4 rat sarcoma cell confirmed the notion of higher and uneven distribution of velocity of FIM in a tumor cell so far shown in color-coded images only. This result and other yet unpublished observations indicate that the velocity and topology of FIM can also contribute to a biological distinction between neoplastic and normal cells. Regular application of the correlation analysis should further expand the study of FIM for its mechanisms and predictive value. Such an approach should be thoroughly examined for a contribution to the knowledge of cancer cells.

This work was supported by grant No. 304/99/0368 from the Grant Agency of the Czech Republic to PV.

Address for reprints:
Pavel Vesely
Institute of Molecular Genetics
Academy of Sciences of the Czech Republic
Flemingovo 2
Prague 6 – Dejvice
166 37 Czech Republic
e-mail: pvy@img.cas.cz

Key words: fast intracellular motion, living cell, video rate confocal laser scanning microscopy, correlation analysis, evaluation of time series of fuzzy images, Brownian motion, cancer cell

PACS: 87.64.T, 87.16, 87.16.U, 05.40.J, 66.10.C

Introduction

Fast intracellular motion (FIM) was originally noticed in live tumor cells (Vesely *et al.* 1993) with a Lasertec 1LM11 60 Hz frame rate red laser scanning confocal microscope (Lasertec Corporation, London, U.K.). Regular study of FIM was made possible only when the original real time true point-by-point confocal laser scanning (Draaijer and Houpt 1988) for reflection imaging, that combined galvanometer mirror scanning for the frame axis with acousto-optic deflection (AOD) scanning in the line direction, became accessible in a video rate confocal laser scanning microscope (VRCLSM) Odyssey (Noran, Middleton, Wisc., USA). Odyssey, with the 488 nm line of argon and later with the 633 nm line of HeNe lasers, offered epi-fluorescence and two reflected light imaging modes, that is, reflected interference contrast (RIC) and backscattered light (BSL) imaging for in vitro (Boyde and Jones 1992, Vesely and Boyde 1996; 2001a,b; Vesely *et al*. 2003) and in vivo in situ (Boyde *et al.* 1998) observation of live cells. Previous studies reviewed by Vesely and Boyde (2001a) have demonstrated the authenticity of FIM and listed the reasons that it could have been revealed by highest spatial and temporal resolution of BSL imaging in the VRCLSM only. Fast intracellular motion has been studied in the cytocenter next to the nuclear space, where the in vitro attached and spread cell is usually thicker than 3 mm. It is best recorded in confocal cross sections <1 mm thick through the space packed with organelles and fibrillar structures (Vesely and Boyde 2001b), all of them involved in complex three-dimensional (3-D) motion. The recorded motion is brought about by trafficking vesicles and particles and translational forces derived from the overall motility of a cell, and modified by contribution of accompanying interference phenomena. The VRCLSM allowed for 3-D mapping of intracellular space for the occurrence of FIM. This 3-D volume was then tentatively de-

fined as an integrated dynamic spatial network (IDSN), which was found out to be larger in neoplastic cells (Vesely and Boyde 1996). Between the IDSN and the cell membrane, which is in contact with the substratum (cover glass), a thin layer appeared, characterized by very fast fluid streaming and a flow of particles represented as white patches. For this appearance it was considered as a communication layer. Recognition of all these compartments on the basis of motility was greatly facilitated by the introduction of the HeNe 633 nm laser, because lower dispersion of red light resulted in deeper penetration into the cells, even in a multilayer, and enhanced the image contrast. In spite of the progress in experimentation, the information about the VRCLSM findings was understandable only in a direct live demonstration in the Odyssey or occasionally in an exceptionally good recording on VHS tape. Communication in print was limited to either short-time sequences of highly unintelligible images or quasi-stereopairs for visualization of motion changes as 3-D sensation. Later, color-coding by combinations of red-green-blue (RGB) images became available (Vesely and Boyde 2001a), which, with video clips, made the PowerPoint presentation of the results acceptable and understandable (Vesely and Boyde 2001b, Vesely *et al*. 2003).

Nonetheless, a numerical quantification of differences in velocities that would complement and improve the current demonstration by color coding has been missing. Standard methods for tracking or pattern recognition could not be applied because of the fuzzy nature of FIM caused by the contribution of interference phenomena to image formation. Other approaches were therefore examined. Finally, the correlation analysis was chosen. When calibrated on Brownian motion and a known type of motion, such as ruffling at the cell margin in comparison with FIM, it proved to hold an explanatory potential that was numerically expressed. Therefore, several incidences of FIM were analyzed, such as in the live K4 cell and after 1 min lasting fixation with 2.5% glutaraldehyde; in cells in the natural tissue context of a green leaf, a plant organ, while fresh and later droopy; during the course of K2 cell reaction to temperature changes; and in normal and tumor cells in mutual contact observed simultaneously. The results of the novel approach to the objective evaluation of time series of fuzzy images featuring the FIM are presented.

Material and Methods

Objects Investigated

Vertebrate Cells: Cultured cells such as the rat K4 sarcoma cells (Vesely 1972), rat K2 fibrosarcoma (Vesely and Weiss 1973), and primary rat embryo fibroblasts were investigated. Live cells were observed in a closed culture chamber in medium (Eagle's MEM w/o phenol red with 10% calf serum) set to physiological pH with nonvolatile 20 mM Hepes buffer.

Plant Cells: A picked green leaf was observed immediately while fresh and later when it became droopy for activity of FIM in plant cells within the natural tissue context. To observe the bottom side of the green leaf, water immersion of the leaf for oil immersion objective lens was mediated by a cup made of stainless steel holding a 0.17 mm thick coverglass separating water immersion of the leaf from the oil immersion of the objective.

Brownian Motion

Diluted milk was placed in 0.17 mm high space between the slide and the coverglass for wide-field microscopy. A few minutes later, after a steady state had been achieved, Brownian motion of milk fat globules was observed in an inverted microscope Nikon Diaphot 300 (Laboratory Imaging Ltd., Prague, Czech Republic) with Nikon LWD 100/0.8 ph dry objective and recorded at real time by a Cohu CCD camera (Cohu Electronics, San Diego, Calif., USA) and a Sony camcorder (Sony Corporation, Park Ridge, N.J., USA). For VRCLSM Odyssey, a Sterilin observation chamber with a 0.5 mm high space under the coverglass was used.

Accommodation of Living Cells in the Microscope

Cells of homoiothermic animals to be examined were seeded onto a 0.17 mm thick, 25 mm dia. round coverglass in a culture dish and grown in 3% CO_2 atmosphere at 37° C. For observation, the coverglass was mounted in a closed double (2.5 mm apart) coverglass chamber with flush-through option. Noran Odyssey was equipped with a cover serving for thermal insulation of the microscope body that was heated to 34° C. For precise maintenance of the vertebrate cells under observation at 37° C, the objective heater large (Bioptechs, Butler, Pa., USA) was employed.

Confocal Microscopy

Video rate confocal laser scanning microscope (VRCLSM) Odyssey (Noran) attached to an upright Nikon Optiphot-2 microscope (160 mm tube length) was used in reflection mode of the red HeNe 633 nm laser with confocal pinhole set to 4 mm unless otherwise specified. The necessary magnification was achieved by combination of Nikon planapo objective ×60/NA 1.4 (oil imm.) with zoom ×5 to ×15. Depending on the distance of the focal plane from the coverglass, the reflection interference contrast (RIC) image in 0–1 μm depth of the cell or deeper in 1–7 μm it was the BSL image that was obtained.

Image Acquisition

Mix video PAL (720×576) output from Noran Odyssey (scanned field 512×480) was digitally recorded onto a Sony Digital8 tape utilizing a Sony DCR-TRV320E PAL

camcorder at full PAL resolution (720×576 pixels) together with on-line recording of the voice protocol of the actual course of the experiment.

Image Information Processing

The Sony Digital8 tape was copied at full PAL resolution (720×576 pixels) together with the recorded voice protocol on a hard disk of the IBM personal computer (PC) with firewire (IEEE 1394) port using Pinnacle Studio DV or later Studio 7 programs. Selected recordings featuring events of interest were optimized for maximum information by adjusting brightness and contrast in the Studio 7 v 7.15.1 program and stored as video clips (MS Windows AVI file) for PowerPoint presentation. Those series chosen for further evaluation by color coding exploiting the RGB composition of three selected subsequent images and for correlation analysis were then cut into 110 individual frames (separated by 1/25 s time interval) and grabbed into MS Windows bitmap format 640×480 pixels.

Spatial and Temporal Resolution in Kinematic Information about Fast Intracellular Motion VRCLSM Versus Wide-Field Microscopy

The VRCLSM Odyssey (Noran) scans at 512 horizontal by 480 vertical pixel resolution with pixel dwell time 100 ns and provides zoom facility.

Spatial Resolution: Analysis of spatial resolution of standard Odyssey visualization of FIM as presented on a display is based on optical parameters given by Nikon planapo objective ×60/1.4 (oil imm.) and HeNe 633 nm red laser. According to Webb and Dorey (1995), this combination gives values of resel (minimum optically resolvable entity on the object) for xy $\text{resel}_{\text{conf}}$=180 nm and for z resel_{z}=682 nm. In respect of Nyquist sampling and/or Kotelnikov-Shannon criterion, stating that for optimum resolution the sampling frequency must be at least 2 to 3 times higher than the frequency observed, the ratio of these frequencies (RF) was calculated for xy $\text{resel}_{\text{conf}}$=180 nm and 512 or 720 horizontal pixels. The result is shown in Table I.

TABLE I Efficiency of image information sampling

X_zoom	Width_µm	No_resels	RF_512	RF_720
1	110	611	0.83	1.17
2	55	305	1.67	2.36
3	37	205	2.49	3.51
5	22	122	4.19	5.9
10	11	61	8.39	11.8
15	8	44	11.63	16.36

Notes
X_zoom = zoom factor
Width__m = picture width in µm
No._resels = number of resels per picture width
RF_512 = ratio of frequencies for 512 horizontal pictures (no. pixels/no. resels)
RF_720 = ratio of frequencies for 720 horizontal pictures (no. pixels/no. resels).

The calculation shows that for zoom X1–X2 the RF is within the range of undersampling while for zoom X3 it is about correct, and from zoom X5 up the valuable oversampling starts. This is in accord with the observations on diatom *Amphipleura pellucida* (Boyde and Jones 1992, Vesely and Boyde 2001a), which showed that full resolution was recognized from zoom X3 up only. The VRCLSM zoom higher than X5 (reaching up to 20 nm/pixel) does not bring in merely the so-called empty magnification. It allows for full use of optical resolution to be achieved for visually clear and comprehensive kinematic information.

Temporal Resolution: The top spatial resolution was not the single important condition for recording the kinematics of the intracellular events in the live cell. The temporal resolution was another important factor. In wide-field microscopy, one exposure in the CCD camera taken at video rate speed lasts equally 40 ms for all pixels in the image compared with only 100 ns pixel dwell time in the Odyssey. It is an X400,000 factor difference in temporal resolution for a pixel. The CCD camera image averages light captured per pixel over 40 ms, while VRCLSM image represents a very sharp section through 40 ms. For fast displacement this has a pronounced effect on the resolution of the visualization of motion.

Correlation Analysis of Time Series of Images Featuring Fast Intracellular Motion

For quantitative determination of the rate of FIM registered in video sequences, computation of the second order correlation coefficient was used.

The correlation coefficient is a normalized measure of the strength of the linear relationship between two variables. Comparison of equivalent data sets has a correlation coefficient of 1, uncorrelated data result in a correlation coefficient of 0, and completely contrary data are indicated by correlation coefficient of –1. The absolute values of the correlation coefficient are within the range (0,1). More detailed information about the correlation analysis can be found in Rektorys (1994) and Cohen *et al.* (2002).

In image processing, the correlation coefficient determines the similarity of images in one series (e.g., time series). Suppose A and B are the digital images or selected areas of an image, that have the same size. The correlation coefficient r between selected areas of interest of the dimension $M*N$ pixels is given by

$$r = \frac{\sum_m \sum_n \left(A_{mn} - \overline{A}\right)\left(B_{mn} - \overline{B}\right)}{\sqrt{\left(\sum_m \sum_n \left(A_{mn} - \overline{A}\right)^2\right)\left(\sum_m \sum_n \left(B_{mn} - \overline{B}\right)^2\right)}},$$

where $\overline{A} = \frac{\sum_m^M \sum_n^N A_{mn}}{MN}$ and $\overline{B} = \frac{\sum_m^M \sum_n^N B_{mn}}{MN}$ are arithmetic averages of image data A and B from the selected areas. On

the basis of characterization of the interdependence of the compared pixels, it is possible to obtain a reasonable criterion for deciding whether important changes are observed.

According to a selection of images to be compared two types of the correlation coefficient were used. The first type (coded c1) is the correlation coefficient *r(t),* which is determined on the grounds of correlation between the image at a given time *t* and the initial image (*t=0*). The second type (coded c2) is correlation coefficient $r_1(t)$, which expresses the dependence between two subsequent in time images *t* and $t+\Delta t$, where Δt is the interval between them.

To compare the development of FIM in various time series of images, each series of 100 images at a 1/25 s interval between frames was evaluated. Both types of correlation coefficient (c1 and c2) were calculated by programs developed for MATLAB (The MathWorks, Natick, Mass., USA). Besides comparison of whole frames also distributed correlation analysis, which is an assessement of rate of image change in several areas within one frame, was made possible.

The choice of a design of c1 and c2 types of the correlation coefficient was motivated by anticipation that c1 will show a continuity of increasing changes in the intracellular situation, while c2 will indicate a coherence of these processes.

For comparing series of images for velocity, mainly least values of c1 were used on the assumption of standard timing (1/25 sec between frames) and lateral magnification.

Results

Calibration of Correlation Analysis

To elucidate the explanatory potential of correlation analysis, Brownian motion of milk fat globules and comparison of K4 cell ruffling with FIM were chosen.

Brownian motion: Brownian motion was studied in the classic model of diluted milk. The movement of fat globules at the steady state under the coverglass was recorded at real time. Both microscopies, that is, wide-field and confocal scanning, were compared.

In wide-field microscopy, a Nikon LWD 100/0.8 ph dry objective was used. The results are pictured in Figure 1. The BM100c1 curve shows fast drop to c1 0.4, indicating very active motion. The BM100c2 curve drops only to c2 0.9, showing the stability of focus and appreciable lack of thermal streaming within the field and time of observation.

In confocal scanning microscopy, a Nikon planapo objective X60/NA 1.4 (oil imm) was used and X1.6 zoom (z1) provided the same lateral magnification as dry Nikon 100x lens, while X10 zoom (z10) offered visualization of Brownian motion comparable with the regular study of FIM. The BMz1c1 curve drops fast to c1 0.2 and stabilizes on c1 0.1 with the BMz1c2 on c2 0.25, which also witnesses stability of the observational parameters. The difference between BM100c1 (c10.4) and BMz1c1 (c1 0.1) curves demonstrates the contribution of the VRCLSM to temporal resolution. Both BMz1 curves are remarkably steady compared with heavily oscillating BMz10c1/c2, of which BMz10c1 drops even to c1 minus values and BMz10c2 oscillates sharply between c2 0.3 and 0.6. This behavior indicates that, at the temporal and spatial resolution of zoom X10, the free Brownian motion is so fast that it surpasses the capturing speed of the technique employed. Therefore, correlation analysis indicates a pattern of chaotic behavior only. For FIM, which is ordinarily studied at zoom X10 or X15, it shows that FIM should be slower than free Brownian motion.

Comparison of velocities of K4 cell marginal ruffling with fast intracellular motion in the cell process behind the ruffling edge (see insert) at X5 zoom: The actively ruffling lamella at the edge of the cellular process of the K4 cell can be observed in real time as an ongoing change of the cell margin if a phase contrast objective of NA ≥0.6 is used. The ruffling motility recorded at the RIC/BSL focus level was compared within one frame with the FIM in the body of the cellular process just behind the ruffling area (Fig. 2) using distributed correlation analysis. It is evident that the "natural" motion of the cell ("natural" because it is already known from other observation techniques) of the ruffle was

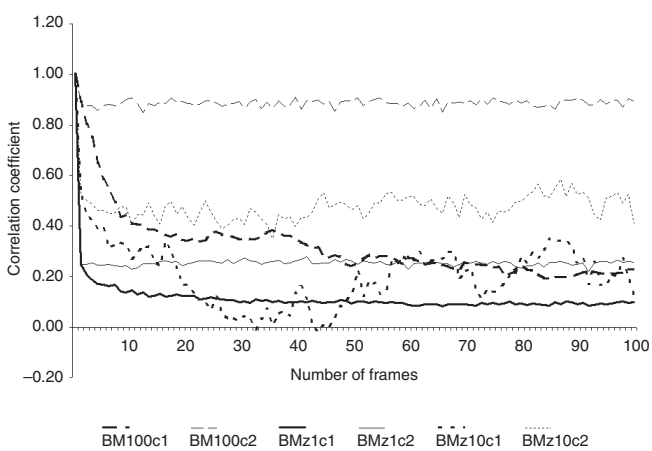

Notes
BM100c1/c2 = wide-field microscopy Nikon LWD 100/0.8 ph dry objective
BMz1c1/c2 = X1 zoom VRCLSM Nikon planapo objective X60/NA 1.4 (oil imm.)
BMz10c1/c2 = X10 zoom VRCLSM Nikon planapo objective X60/NA 1.4 (oil imm.)

FIG. 1 Velocity of Brownian motion of fat globules in diluted milk. Brownian motion was studied in the classic model of the movement of milk fat globules at the steady state under the coverglass at room temperature. In scanning microscopy (Nikon planapo objective X60/NA 1.4 (oil imm.), zoom (z1) X1.6 was used to provide the same lateral magnification as wide-field microscopy (Nikon 100x dry lens). Zoom (z10) X10 gave a scale of visualization of Brownian motion comparable to that regularly employed in the studies of fast intracellular motion.

faster (c1 0.2) than FIM in the body of the cellular process (c1 0.4). The ruffle was also faster than the live FIM (c1=0.3) from Figure 3 (X10 zoom). The FIM activity in the body of the cellular process was slower than the ruffle, yet appears comparable with the course of FIM activity in the K2 cell (Fig. 4, X15 zoom), which was recorded at the BSL focus level deeper in the cell. In spite of a difference in zoom factors and the focus plane levels, the curves of c1 and c2 display similarity and continuity in all the cases. This finally calibrated correlation analysis for use as a measure of velocity of fast intracellular motion from time series of fuzzy images.

Quantification of Fast Intracellular Motion Using Correlation Analysis

Correlation analysis was then applied to several instances of FIM waiting for cautious evaluation. These were FIM in living and dying states, influence of temperature on FIM, and comparison of FIM in a normal and in a neoplastic cell. In all graphs showing the time course of the correlation coefficients, their original values were used. However, for Tables II and III, a complement of correlation coefficients to 1 (i.e., 1 - c1 or c2) was chosen for better intuitive appreciation of the change of velocity of FIM (expressed in percent) at selected times.

Assessment of the rate of change of fast intracellular motion in living and dying states: Two biological situations served to study the difference in the observed velocity of FIM in a living and an early dying biological subject (Fig. 3). These were an in vitro cultured animal cell before and immediately after fixation and a plant cell in situ in a green leaf, an organ of the plant, when fresh and droopy 2 h later.

The same space with FIM inside the rat sarcoma cell K4

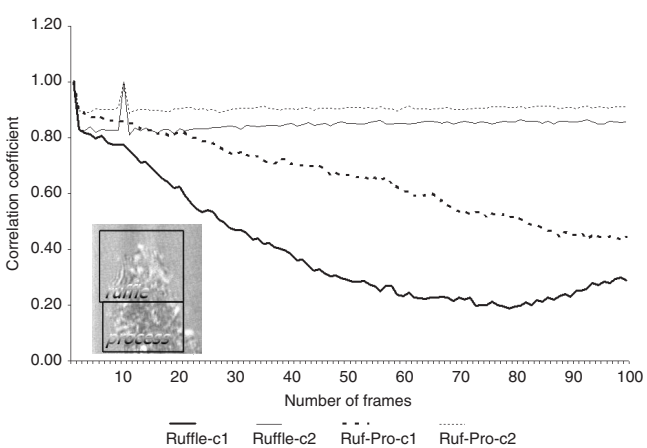

Notes
Ruffle-c1/c2 = actively ruffling lamella at the edge of the K4 cell (upper insert)
Ruf-Pro-c1/c2 = activity of the cell process behind the ruffle (bottom insert)

FIG. 2 Comparison of velocities of ruffling and fast intracellular motion in the cell process behind the ruffling edge at X5 zoom. Two areas from the same image were selected. The actively ruffling edge of the cellular process of the K4 cell (upper insert) was compared with the activity in the body of the cellular process just behind the ruffling area (bottom insert) at the RIC/BSL focus level.

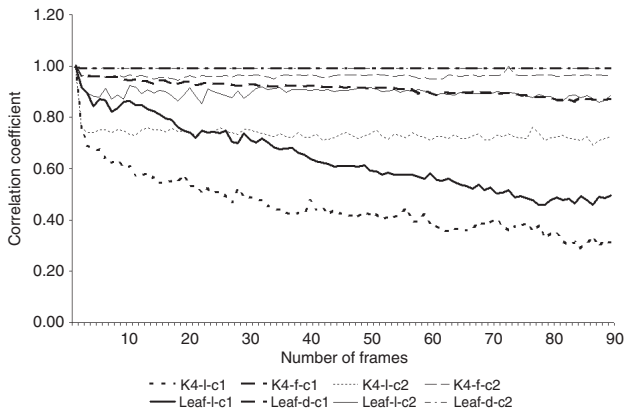

Notes
K4-l-c1/c2 = K4 cell live c1, c2
K4-f-c1/c2 = K4 cell fixed c1, c2
Leaf-l-c1/c2 = Green leaf live c1, c2
Leaf-d-c1/c2 = Green leaf droopy c1, c2

FIG. 3 Difference in velocity of fast intracellular motion (FIM) in living and dying states (X10 zoom). Two biological situations were used to learn if there is a difference in the observed velocity of FIM in a living and an early dying biological subject. The in vitro cultured animal cells before and early after fixation as well as plant cells in situ on the bottom surface of a green leaf (plant organ) while fresh and later droopy were examined.

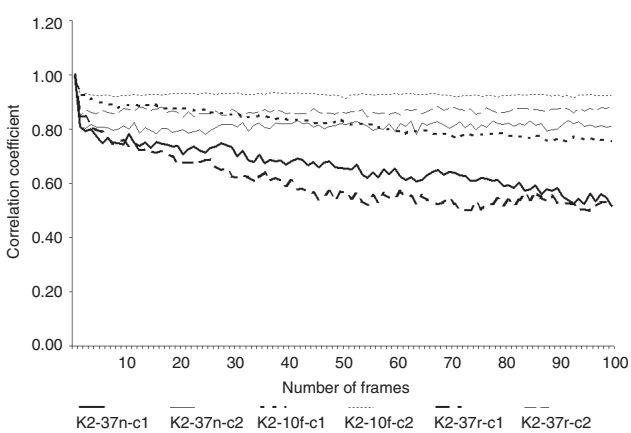

FIG. 4 The velocity of fast intracellular motion (FIM) observed in living K2 cells at 15X zoom depends on the temperature. Rat fibrosarcoma K2 cells in eutrophic culture conditions were observed in the cytocenter for temperature-dependent changes of velocity of FIM. K2 cells were investigated at standard 37° C (K2-37n-c1/c2), then at room temperature (21° C) immediately after 5 h of cooling in a refridgerator at 10° C (K2-10f-c1/c2) and then at 37° C after 22 h of rewarming up back at 37° C (K2-37r-c1/c2).

TABLE II Comparison of mutual changes of velocity of fast intracellular motion (FIM) caused by temperature shifts

Data	K2-37n-c1	K2-10f-c1	K2-37r-c1	K2-37n-c2	K2-10f-c2	K2-37r-c2
CC	0.61	0.78	0.52	0.83	0.92	0.87
1 – CC	0.39	0.22	0.48	0.17	0.08	0.13
% of 37n	100	56	123	100	47	76

Notes:
Data=correspond to Figure 4 at 3 s of recording
CC=correlation coefficients c1 or c2
1 – CC=complement of CC (1 – c1 or c2)
% of 37n=% of decreased or increased rate of change of FIM in the experimental situation 10f and 37r compared with standard 37n calculated from the complement of CC.

at the 2–3 micron distance from the coverglass was recorded at X10 zoom for the live cell in optimum cell comfort and during through-flush fixation with 2.5% glutaraldehyde in phosphate-buffered saline (PBS). Two phases of the process were analyzed: live cell, and then 1 min later after starting the fixation. A fast and steady drop of c1 for the live cell to values <0.4 and drop and leveling of c2 just <0.8 were in sharp contrast with values >0.9 for c1 and c2 in the cell soon (1 min) after the beginning of fixation.

Plant cells in situ in the surface layer on the bottom side of the green leaf were investigated at room temperature (21° C). Fast intracellular motion resembling microcirculation around the cytocenter was found even at zoom <×5. It was recorded at ×10 zoom in a freshly picked leaf and in a leaf becoming droopy after 2 h in the dark without water. Although there was no visible difference, and the droopy leaf did not seem to be dry, a very similar increase of the c1 and c2 for the droopy leaf was observed as for the fixed K4 cell. It should be emphasized that this slowdown of FIM in the leaf was found without artificial intervention such as fixation. There was no microscopic evidence of a shape change or absence of water in the plant cells observed.

Investigation of the influence of temperature changes on the velocity of fast intracellular motion observed at X15 zoom in live K2 cells: The velocity of FIM in the cytocenter outside the nucleus of rat fibrosarcoma K2 cells in eutrophic culture conditions was investigated at standard 37° C, then at room temperature (21° C) immediately after 5 h of cooling in a refridgerator at 10° C, and then at 37° C after 22 h of warming up back at 37° C (Fig. 4). While at original 37° C, the c1 reached 0.6; after cooling, it rose up to almost 0.8 and on rewarming it dropped down to 0.5 slightly below the original value. The exact comparison of these changes is shown for time 3 s after the beginning of recording in Table II in percent. The percentage is calculated from the complement of correlation coefficient to 1, which better expresses the mutual changes of what can be considered as a measure of velocity of FIM. The behavior in rewarming conditions can be seen as a reaction of hypercompensation. Although the values of c2 behaved in a standard way (also confirming the stability of focus), they proportionally followed the pattern of c1.

The Higher Velocity of Fast Intracellular Motion with a Tumor Compared with Normal Cell is Confirmed by Distributed Correlation Analysis

A rat sarcoma cell (K4) and an adjacent normal rat fibroblast (LWF) living in eutrophic conditions at 37° C were recorded for the activity of FIM about 1.5 mm apart from the coverglass in BSL mode at X5 zoom. The areas of interest indicated by RGB color coded picture (Fig. 5) were selected in Figure 6 to match comparative locations in the cells observed, that is, A–D, B–E, C–F. The distribution of activities defined by correlation analysis is given in Figure 7. For lucidity of presentation, only c1 is pre-

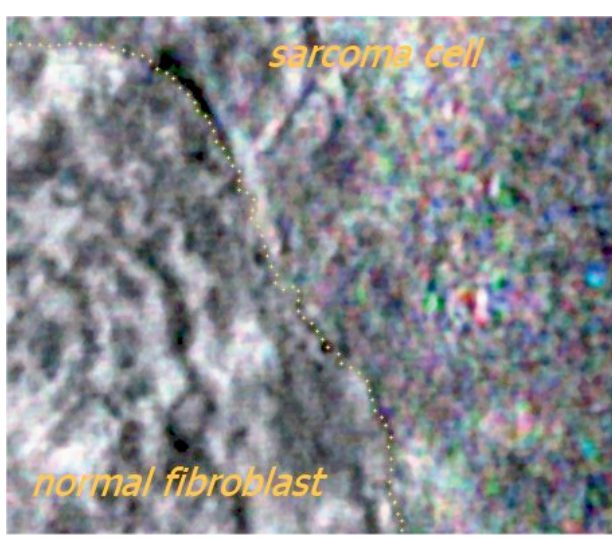

FIG. 5 Higher velocity of fast intracellular motion (FIM) in a rat sarcoma cell compared with a normal rat fibroblast is shown in adjacent (cell borders: dotted yellow line) peripheral areas using color combination from red-green-blue (RGB). Three sequential time frames 1/25 s apart are combined in color, each with arbitrary time zero = red, next = green, last = blue. The greater the deviance from pure whiteness, the more has a reflective feature moved. It will be seen that the fibroblast is less colored than the sarcoma cell, suggesting higher velocity of FIM in the tumor cell than in the normal cell, even along thin cell peripheries. While the fibroblast shows a rather uniform distribution of motion, the sarcoma cell displays foci of enhanced activity of FIM. The observation was numerically confirmed by correlation analysis. Nikon planapo objective X60/NA 1.4 (oil imm.), zoom X5, picture width 22 μm.

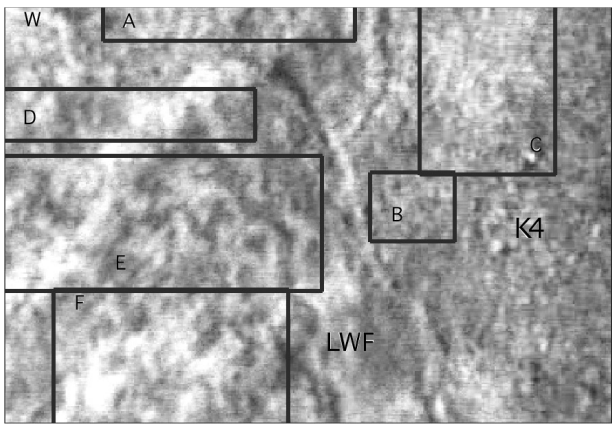

FIG. 6 A rat sarcoma cell (K4) adjacent to a normal rat fibroblast (LWF) observed at 5X zoom (see Fig. 5 for color combination from red-green-blue [RGB]. Areas (K4: A B C; LWF: D E F) sampled for comparison of velocities of fast intracellular motion shown in Figure 7 are represented by a diagram.

Description of the areas: A=narrow peripheral area of the sarcoma cell close to the contact with the fibroblast; B=peripheral area of the sarcoma cell extending deeper inside the cell; C= focus of maximum activity (see Fig. 5) inside the sarcoma cell; D= narrow peripheral area of the fibroblast close to the contact with the sarcoma cell (analogous to A); E=peripheral area of the fibroblast extending deeper inside the cell (analogous to B); F=focus of maximum activity (see Fig. 5) inside the fibroblast (analogous to C); W=the whole image.

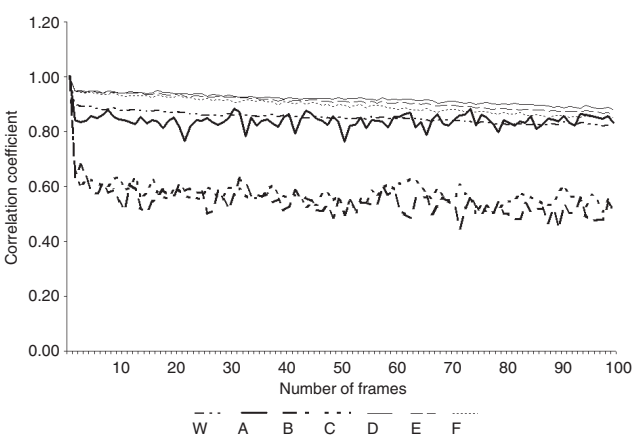

FIG. 7 Evaluation by distributed correlation analysis confirms higher and uneven velocity of fast intracellular motion (FIM) in the neoplastic K4 cell. Only c1 curves are shown. Curve W gives the average value over the whole image and demonstrates how important for true analysis is to be able to compare activities in selected areas. In the sarcoma cell K4, the B and C are foci of very high activity as visualized in Figure 5 and manifest c1 dropping down to 0.5. The registered activity can be partly caused by the thickness of the K4 cell. However, comparison of c1 in areas D for the fibroblast and A for the sarcoma cell, both from adjacent thin cell edges, shows a smooth curve (c1: 0.92-0.88) for the fibroblast and an agitated curve (c1: 0.84-0.83, oscillating between 0.89 and 0.76) for the tumor cell. Thus, a noticeably higher velocity and uneven distribution of FIM in the tumor cell are clearly evident.

TABLE III c1 data from Figure 7 (presented as a complement of c1) show higher activities in A, B & C areas

Time _sec	W	A	D	B	E	C	F
0	0	0	0	0	0	0	0
1/25	0.1	0.16	0.05	0.37	0.05	0.35	0.06
1/5	0.12	0.15	0.05	0.42	0.06	0.38	0.06
2/5	0.12	0.16	0.06	0.49	0.06	0.41	0.07
1	0.14	0.18	0.07	0.42	0.07	0.44	0.08
2	0.15	0.18	0.08	0.48	0.09	0.5	0.1
3	0.17	0.17	0.1	0.5	0.12	0.49	0.13

Notes:
Time_sec=time in s from the beginning of evaluation
W, A-D, B-E, C-F=letters corresponding to areas in Figures 5,6
A/D, B/E, C/F=pairs indicating concurring areas

sented because the standard behavior of c2 confirmed the stability of focus. Curve W gives the average value over the whole image and demonstrates the importance of comparing activities in selected areas of the same image. In the sarcoma cell K4, the B and C are foci of very high activity as visualized in Figure 5, which shows c1 dropping down to 0.5. The registered activity can be partly caused by the thickness of the K4 cell. However, comparison of c1 in areas D for the fibroblast and A for the sarcoma cell, both located along thin cell edges, shows a smooth curve (c1: 0.92–0.88) for the fibroblast and an agitated curve (c1: 0.84–0.83, oscillating between 0.89 and 0.76) for the tumor cell. Thus, a noticeably higher velocity and uneven distribution of FIM in the tumor cell are clearly evident.

In Table III, numerical values of the complement of c1 picked up at six selected time intervals demonstrate the difference between the whole image and compared twin areas (W, A–D, B–E, D–F). There is evidence of difference already after 1/25 s and within 1 s it reaches almost the maximum. Hence, the investigation of a cell for FIM over only 1 s can provide very substantial information about the rate of change of FIM and its topological distribution. The analyzed case numerically confirmed the earlier impression from color coded image in Figure 5.

Three sequential time frames 1/25 s apart are combined in color, each with arbitrary time zero = red, next = green, last = blue. The greater the deviance from pure whiteness, the more has a reflective feature moved. It will be seen that the fibroblast is less colored than the sarcoma cell, suggesting higher velocity of FIM in the tumor cell than in the normal cell, even along thin cell peripheries. While the fibroblast shows a rather uniform distribution of motion, the sarcoma cell displays foci of enhanced activity of FIM. The observation was numerically confirmed by correlation analysis. Nikon planapo objective X60/NA 1.4 (oil imm.), zoom X5, picture width 22 mm.

Discussion

Correlation analysis allowed for evaluation of time series of fuzzy images. It determines that, in the case where

we observe two processes (images) which are strongly linearly dependent either in a positive or negative way, then the absolute value of the correlation coefficient is large (near 1). In other words, the more similar characteristics the processes (images) have the larger is the correlation between them. On the other hand, if two processes (images) develop differently, then the correlation coefficient is small (near 0). Completely contrary data, which are indicated by correlation coefficient of up to –1, signify for a time series of images an occurrence of a sharp discontinuity in the process observed. Such event testifies for lower frequency of data (image) collection than adequate according to Kotelnikov-Shannon criterion if applied to a genuine frequency of the process studied. The two types of the correlation coefficient (c1 and c2) proved to show trend and magnitude of an increasing overall change (c1) and stability and adequacy of the change at each step (c2). Tables II and III show that for characterization of velocity of time series of fuzzy images of FIM 10-25 images taken at video rate should be sufficient. In the reported experiments, the successful calibration of correlation analysis permitted adding a numerical measure to FIM. This made several meaningful comparisons of FIM possible.

The correlation analysis showed the benefit of time resolution of the VRCLSM in capturing Brownian motion compared with wide-field microscopy (Fig. 1). In the same experiment, the evaluation of the X10 zoom imaging of simple Brownian motion demonstrated that its speed was beyond time resolution of even the VRCLSM. This finding provided an argument against viewing slower FIM as a simple Brownian motion. Comparison of FIM with the activity of a marginal ruffle (Fig. 2) calibrated FIM into the velocity range of recognized cellular motilities.

The correlation analysis then brought evidence (Fig. 3) about the similarity between the cessation of activity of FIM in a K4 cell being fixed in vitro and ceasing FIM naturally in cells of a green leaf becoming droopy in situ. Exposure of eutrophic K2 cells to cold and then rewarming (Fig. 4) was designed to discover whether the velocity of FIM—because it was generally considered a simple Brownian motion—behaves accordingly. The result provided strong evidence against this assumption, because, while in theory the difference in speed after this cooling should be limited to 3% (Bray 2001), it dropped down for c1 to 56%, then shot up to 123% on rewarming (Table II). Although these percentages are difficult to reconcile, 3% change of velocity is hardly possible to spot, while the retardation and later acceleration of FIM were in this case clearly seen.

Finally, the distributed correlation analysis was applied to compare FIM in corresponding areas of a normal fibroblast with a sarcoma cell in contact and imaged in one frame (Figs. 5,6). The numerical values of c1 confirmed the notion of higher and more uneven distribution of velocity of FIM in the tumor cell (Fig. 7), which so far has been indicated only by color-coded visualization (Fig. 5). Such a contrast in the velocities of FIM cannot be merely caused by the thickness of the K4 cell, since the differences are also found along the thin cell edges. Possible involvement of the mechanism of contact inhibition of locomotion (Vesely and Weiss 1973) is rather ruled out as the mutual contact had persisted already for several hours. The analyzed case numerically confirmed the earlier idea about the nature of tumor cells, which was already gained from numerous unpublished live observations on the screen of Odyssey, and later made demonstrable by color-coded images such as in Figure 5.

This result indicates that besides the larger extent of the IDSN (Vesely and Boyde 1996), the velocity and topology of FIM could contribute to a biological distinction between normal and cancer cells. For elucidating this assumption a regular application of correlation analysis can expand the knowledge of FIM if done within a framework of carefully designed experiments.

Therefore, it appears imperative to list the necessary precautions in performing experiments using VRCLSM reflection imaging of living cells for obtaining data for correlation analysis. The main issues are the stability of scanning and focus, and the distinct location of the observed area inside the 3-D space of the cell.

The scanning and focus should be tested before every experiment. We inspected a flat piece of polished aluminum equilibrated to the desired temperature in reflection mode at ×10–15 zoom with an objective of at least NA 1.2, so that the microporosity of the surface was clearly recognized. Any image change like "waving" or "motion" indicates problems with scanning, and "breezing" signifies an interference pattern generated by instability of focus. During the experiment and in recordings, a running control of focus stability was provided by the focused cell periphery in contact with the underlying substratum and the observation of stability of interference fringes generated by side slopes of a cell. It was the introduction of the HeNe red laser that allowed for recognition of the acoustic interference, which from time to time caused scanning disturbance when the Argon 488 nm laser was used. Apparently, the acoustic waves generated by the air-cooling system could influence the AOD of Odyssey.

For fair location of the area of interest inside the cell it is necessary to keep in mind that the confocal axial resolution leads up to a stratification of imaging of the living cell 3-D interior. The confocal section less than 1 μm thick (Odyssey with pinhole 4 mm and objective 60/1.4) shows the RIC image of cell-to-substratum contacts up to about 1 mm depth into the cell while deeper the BSL image is obtained, quality of which depends on a part of cell anatomy inspected. Inside the thin peripheral lamella (1-3 mm thick) trafficking particles are pictured similarly to ordinary phase or differential interference contrasts only with higher axial resolution. In the area of thick cytocenter outside the nucleus no structural information is given just FIM is revealed. Inside the nucleus much faster motion of white patches is usually observed and an impression of streaming of liquid is perceived. Above the cytocenter

on top of a cell only fast motion of waving cell surface features is seen.

There are two opposite concepts of the origin of FIM. Generally, FIM is at first sight regarded as Brownian motion. This view takes a cell for a bagful of organelles and molecules freely moving and interacting with one another, which is overlooking the fact that the cytocenter of the in vitro attached and spread cell is crowded with organelles, fibers and lamellae organized into a structure. Hardly any free space for classic Brownian motion is left. Unfortunately, there are only few experienced experimenters with FIM because of a lack of adequate instrumentation. For them it appears that FIM results from complex 3D motion in the cytocenter, which is mainly driven by transport of large molecules, trafficking of vesicles, and translational forces derived from motility of the whole cell. Interference phenomena arising on these intricate tubulo-membraneous structures of the cytocenter amplify any motion of real tiny particles, whose size can be far below the optical resolution, and thus contribute to a fuzziness of the images of FIM.

Current experiments confirmed that simple Brownian motion is faster than FIM, which corresponds to our previous observation that FIM was slower than bound Brownian motion exhibited by freely waving cell surface projections (Vesely and Boyde 2001a,b). It is obvious that the complex causes of FIM naturally include the random thermal motion of water molecules, which drives the so-called Brownian motion phenomena such as Brownian linear or rotary ratchets (Peskin *et al*. 1993, Erdmann *et al.* 2002), a streaming in narrow spaces influenced by properties of guiding structures (Caspi *et al.* 2000), and a power of supramolecular springs and ratchets (Mahadevan and Matsudaira 2000). Also all these phenomena are now becoming amenable to comparative investigation for the role they play in the cell, that is, in a living and functional biological entity.

Although the present form of correlation analysis advanced the objective evaluation of FIM, further tasks should be tackled. In the reflection imaging, even with a high probability that real vesicles or particles will be seen, they are imaged only as patches, usually white. The next steps in the evaluation of FIM should be the determination of prevailing direction of the trafficking patches and also of the direction of apparent fluid streaming, which is biased by the way the scanning is technically performed. A simple tracking of individual patches would be not only laborious, but also severely limited by problems of identification. In this respect it would also be desirable to relay our current approach to multiple-particle-tracking microrheology (Tseng *et al.* 2002) and compare it with results of laser-tracking microrheology (Yamada *et al.* 2000) and measurements of the viscoelastic properties of the cytoplasm using ferromagnetic beads (Bausch *et al.* 1999).

There is a promising future for extending the investigations of living cells using VRCLSM complemented with correlation analysis. In spite of the termination of Noran's production of confocals and lack of reflection imaging in the otherwise superior Yokogawa's confocal scanner there will be new instrumentation soon. A new clone of VRCLSM of the design invented by Draaijer and Houpt (1988) has been announced to appear. It will be the Vt^{eye} from VisiTech International, Ltd., Sunderland, UK, which should replace Noran Odyssey, Odyssey XL, and OZ already in 2004. Next progress in the analysis of FIM can be achieved by tracing labeled particles on the background of FIM. This should become possible with a confocal microscope, which will use resonant galvanometer for line scan. It will enable simultaneous fluorescence and reflection imaging at different wavelengths while avoiding cross bleaching. Such an instrument was originally developed in R.Y. Tsien's lab (Tsien and Bacskai, 1995). Later, it was reproduced commercially by Nikon in VRCLSM RCM-8000, in which the reflection mode was, unfortunately, omitted. Hopefully, an innovation of confocal microscope to this level of performance and also complemented with the phase contrast and DIC confocal facility (Zeiss LSM 510) will come up soon.

Conclusions

The introduction of correlation analysis upgraded the VRCLSM observation of fast intracellular motion (FIM) in live cells to a promising tool for tackling several issues in cell biology. Now, the driving force of the random thermal motion of water molecules, which underlies the so-called Brownian motion phenomena, can be directly examined for the role it plays in the intracellular events. Examination of FIM by VRCLSM evaluated by correlation analysis is becoming an independent noninvasive investigation of the topical organization and overall and/or local instantaneous reactions of cells elicited by general and/or specific stimuli. It is ready to be exploited in an in vitro comparative study of neoplastic versus normal cells for rapid changes of behavior and also for probing cancer cells in situ in fresh tumor biopsis.

References

Bausch AR, Moller W, Sackmann E: Measurement of local viscoelasticity and forces in living cells by magnetic tweezers. *Biophys J* 76, (1 Pt 1), 573–579 (1999)

Boyde A, Jones SJ: Real time confocal microscopy. *Binary Comp Microsc* 4, 119–123 (1992)

Boyde A, Capasso G, Unwin RJ: Conventinal and confocal epi-reflection and fluorescence microscopy of the rat kidney in vivo. *Exp Nephrol* 6, 5, 298–408 (1998)

Bray D: *Cell Movements from Molecules to Motility*, 2nd ed. Garland Publishing, London (2001) 4–5

Caspi A, Granek R, Elbaum M: Enhanced diffusion in active intracellular transport. *Phys Rev Lett* 25, 85, (26 Pt 1), 5655–5658 (2000)

Cohen P, Cohen J, West SG, Aiken L S: Applied multiple regression/correlation analysis for the behavioral sciences, 3rd ed. Lawrence Erlbaum Associates, Mahwah, NJ (2002)

Draaijer A, Houpt PM: A standard video-rate confocal laser-scanning reflection and fluorescence microscope. *Scanning* 10, 139–145 (1988)

Erdmann U, Ebeling W, Anishchenko VS: Excitation of rotational modes in two-dimensional systems of driven Brownian particles. *Phys Rev E Stat Nonlin Soft Matter Phys* 65, (6 Pt 1), 061106 (2002)

Mahadevan L, Matsudaira P: Motility powered by supramolecular springs and ratchets. *Science* 7, 288, (5463), 95–100 (2000)

Peskin CS, Odell GM, Oster GF: Cellular motions and thermal fluctuations: the Brownian ratchet. *Biophys J* 65, 1, 316–324 (1993)

Rektorys K: *Survey of Applicable Mathematics,* 2nd ed. Kluwer Academic Publishers, Dordrecht, Germany (1994)

Tseng Y, Kole TP, Wirtz D: Micromechanical mapping of live cells by multiple-particle-tracking microrheology. *Biophys J* 83, 6, 3162–3176 (2002)

Tsien RY, Bacskai BJ: Video-rate confocal microscopy. In *Handbook of Biological Confocal Microscopy,* 2nd ed. (Ed. Pawley JB) (1995) 459–478

Vesely P: Tumour cell surface specialization in the uptake of nutrients evidenced by cinemicrography as a phenotypic condition for density independent growth. *Folia Biologica (Praha),* 18, 395–401 (1972)

VeselyP, Boyde A: Video rate confocal laser scanning reflection microscopy in the investigation of normal and neoplastic living cell dynamics. *Scan Microsc Suppl 10*: 201–211 (1996)

Vesely P, Boyde A: Fast intracellular motion in the living cell by video rate reflection confocal laser scanning microscopy. *J Anat* 198, 641–649 (2001a)

Vesely P, Boyde A: Red laser video rate confocal reflection imaging for high spatial and temporal resolution study of intracellular motion. (abstr.) *Scanning* 23, 84 (2001b).

Vesely P, Weiss RA: Cell locomotion and contact inhibition of normal and neoplastic rat cells. *Int J Cancer* 11, 64–76 (1973)

Vesely P, Jones SJ, Boyde, A: Video-rate confocal reflection microscopy of neoplastic cells: rate of intracellular movement and peripheral motility characteristic of neoplastic cell line (RSK4) with high degree of growth independence in vitro. *Scanning* 15, 43–47 (1993)

Vesely P, Mikš A, Novák J, Boyde A: Evaluation of pattern of fast intracellular motion (FIM). (abstr.) *Scanning* 25, 2, 56 (2003)

Yamada S, Wirtz D, Kuo SC: Mechanics of living cells measured by laser tracking microrheology. *Biophys J* 78, 4), 1736–1747 (2000)

Webb RH, Dorrey CK: The pixelated image. In *Handbook of Biological Confocal Microscopy, 2nd ed.* (Ed. Pawley JB) (1995) 55–67